Catal Lett (2017) 147:572–580
DOI 10.1007/s10562-016-1959-3

Study of Catalyst Deactivation in Liquid-Phase Hydrogenation of 3-Nitrostyrene Over Au/Al_2O_3 Catalyst in Flow Reactor

A. L. Nuzhdin[1] · S. I. Reshetnikov[1] · G. A. Bukhtiyarova[1] · B. L. Moroz[1,2] · E. Yu. Gerasimov[1,2] · P. A. Pyrjaev[1] · V. I. Bukhtiyarov[1,2]

Received: 26 October 2016 / Accepted: 20 December 2016 / Published online: 12 January 2017

Abstract For the first time, we report the results of the study of dynamics of the Au/Al_2O_3 catalyst deactivation during the selective liquid-phase 3-nitrostyrene (3-NS) hydrogenation in a fixed bed flow reactor. It is shown that the formation of carbonaceous deposits is the main reason of catalyst deactivation, while the leaching of gold from the Au/Al_2O_3 catalyst or enlargement of the gold particles has not been detected. The content of the carbon deposits on the spent catalyst at the inlet of the reactor is higher than at the outlet and increases as the initial concentration of 3-NS grows. The character of carbonaceous deposits allocation and analysis of reaction products point out to 3-vinylnitrosobenzene as the main source of the Au/Al_2O_3 catalyst deactivation coinciding with the speculation arising from the kinetic modeling.

Graphical Abstract

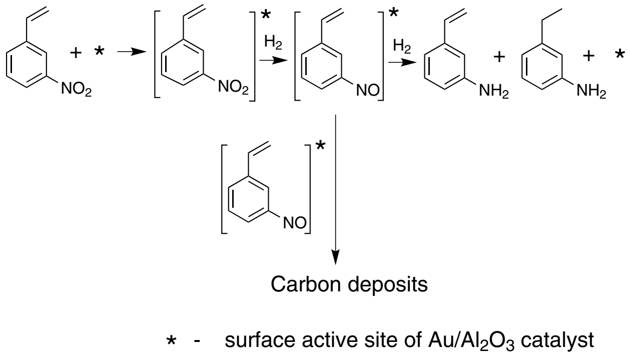

Keywords Heterogeneous catalysis · Deactivation · Liquid-phase hydrogenation · Selective hydrogenation · Kinetic modeling · Au/Al_2O_3 catalyst · 3-Nitrostyrene · Flow reactor

1 Introduction

Functionalized anilines are commercially important intermediates in the manufacture of agrochemicals, pharmaceuticals, and other chemical products [1–3]. Conventional techniques for their production are based on the reduction of a nitro group in a corresponding substrate with stoichiometric amounts of reducing agents, such as iron in acid media (Bechamp process), H_2S, or NaHS. These processes produce a large amount of harmful wastes and display low selectivity for the reduction of a nitro group in the presence of other reducible groups such as C=O or C=C bonds, both reasons restrict their use in practice [3]. In accordance with a current trend to use atom economy methods in organic synthesis, the selective reduction of nitro groups

✉ A. L. Nuzhdin
anuzhdin@catalysis.ru

[1] Boreskov Institute of Catalysis SB RAS, Lavrentieva Ave., 5, Novosibirsk, Russia 630090

[2] Novosibirsk State University, Pirogova Str., 2, Novosibirsk, Russia 630090

with hydrogen over heterogeneous catalysts has been highlighted as a promising route for the development of a new, environmentally friendly technology for the production of functionalized anilines [3–5]. The preferential reduction of a nitro group in the presence of C=C bond is not so straightforward because of high reactivity of this functionality toward metal-catalyzed hydrogenation [3]. Catalytic metals (e.g., Pt, Ru, and Ni), which are most widely used for the hydrogenation of organic molecules, hardly provide the selective reduction of nitro groups when carbon–carbon double bond is present in the same molecule, although adjustment of the solvent, catalyst support, and amount of noble metal, as well as the addition of modifiers can contribute to success in certain cases [3, 6–8]. In the last decade, heterogeneous catalysts comprising monometallic Pt [3, 6, 7], Ru [7], Ni [7], Au [6, 7, 9–13], Ag [14, 15], Mo [16], or bimetallic Au–Pt [17] and Pt–Zn [18] nanoparticles were proposed for selective hydrogenation of 3- or 4-nitrostyrene, which are used most often as model compounds containing both nitro-group and C=C bond. It has been shown that supported gold nanoparticles demonstrate one of the highest selectivity toward the nitro group hydrogenation and produce the corresponding aromatic amine with high yield [5–7, 9–13].

It has been observed that the supported gold catalysts lose their activity during liquid-phase or gas-phase hydrogenation of aromatic nitro-compounds [9, 12, 19–24], but the publications considering the reasons for this are still scarce. Aggregation of the gold nanoparticles was assumed as a main reason for a decrease in the 4-chloronitrobenzene (4-CNB) conversion over the Au/ZrO_2 catalyst in successive batch-mode experiments using ethanol as a solvent [20]. A decline in the activity of the Au/Al_2O_3 and Au/TiO_2 catalysts for nitrobenzene hydrogenation detected after their recycling was also explained by sintering of gold nanoparticles [21]. On the contrary, no enlargement of the gold particles was observed in the continuous gas-phase hydrogenation of 4-CNB to 4-chloroaniline over the Au/Al_2O_3 catalyst [19]. The authors established that blocking of the active sites via deposition of carbon was a cause of temporal deactivation of the Au/Al_2O_3 catalyst.

Generally, hydrogenation of aromatic nitro compounds is performed in either liquid-phase batch reactors or gas-phase flow reactors. Meanwhile, the use of three-phase flow reactor allows an improvement of gas-liquid-solid interaction and reduction of the side products through a better control over process variables [25–28]. Besides, carrying out the reactions in fixed bed flow reactor makes it possible to monitor the changes in catalytic activity and selectivity with time-on-stream and to reveal the dynamics of catalyst deactivation.

Recently, we observed [12] a highly selective hydrogenation of several substituted nitrobenzenes, such as 2-, 3-, and 4-CNBs; 3-nitrostyrene (3-NS) and 4-nitroacetophenone over the Au/γ-Al_2O_3 catalyst to the corresponding anilines at 60–110 °C and 1.0 MPa in a three-phase packed-bed reactor operating in the up-flow mode. One important result found was that hydrogenation of 3-NS led to the formation of 3-vinylaniline (3-VA) with selectivity of up to 93% at substrate conversion exceeding 98%. However, a smooth deactivation of the catalyst with time on-stream was observed mainly due to the appearance of carbonaceous deposits.

Therefore, the objective of the present work is to study the dynamics of the Au/γ-Al_2O_3 catalyst deactivation during 3-NS hydrogenation in a liquid-phase packed bed flow reactor as a function of the inlet 3-NS concentration. The allocation of carbon deposition along the reactor length depending on the initial 3-NS concentration has been also examined.

2 Experimental

2.1 Chemicals

Hydrogen tetrachloroaurate H[$AuCl_4$]·aq (49.47 wt% Au) from Aurat (Russia) was used as the source of gold to prepare the gold catalyst. 3-Nitrostyrene (Acros Organics, 97% pure) was used as the reagent for catalyst testing. Toluene of 99.5% purity from “ECOS” (Russia) and *n*-decane (>99% pure) from Acros Organics were employed for catalytic experiments as solvent and internal gas chromatography (GC) standard, respectively.

2.2 Catalyst Preparation

As the catalyst support, we used γ-Al_2O_3 (BET specific surface area, 215 m^2 g^{-1}, total pore volume, 0.61 cm^3 g^{-1}, mean pore diameter, 9.6 nm) prepared by extrusion of a paste consisting of aluminum oxide of Puralox TH 100/150 grade and aluminum hydroxide of Pural SB grade (both produced by Sasolchemie GmbH, Germany) mixed in a ratio of 30:70 by weight and added with an aqueous solution of nitric acid as a peptizing agent. The cylindrical Al_2O_3 granules of 1.5 mm in diameter thus obtained were dried at 110 °C overnight and calcined in a flow of air at 550 °C for 4 h. Then they were crushed and sieved, the grains of 250–500 μm in diameter were used for the catalyst preparation. The support was dried at 110 °C in a drying oven for 8 h immediately before gold deposition. The Au/Al_2O_3 catalysts were prepared through the adsorption of anionic gold(III) hydroxychloride complexes onto the alumina support from an aqueous solution of H[$AuCl_4$] + NaOH at 70 °C and pH = 7 (the so-called “deposition–precipitation technique”) followed by washing with distilled water, drying and calcining in air at 400 °C, as described earlier [29]. Afterwards, the final sample was calcined at 600 or 800 °C. As a result of this procedure, a set of the Au/Al_2O_3 catalysts containing 1.8–1.9 wt% of Au with the different mean diameters of supported gold nanoparticles was obtained (d_l = 2.1 ± 0.4, 2.8 ± 0.6 and 5.7 ± 1.5 nm).

2.3 Catalyst Characterization

The gold content of the fresh and spent catalyst samples was measured *in vacuo* by using the X-ray Fluorescence (XRF) technique on an ARL instrument equipped with a Rh anode (X-ray tube voltage, 50 kV, tube current, 40 mA, exposure time, 10 s). Transmission electron microscopy (TEM) studies were performed with a JEM-2010 (JEOL, Japan) electron microscope with a lattice resolution of 0.14 nm and a 200 kV accelerating voltage. The mean diameters (d_l) of gold particles for each catalyst sample were determined by counting over 300 particles in TEM images taken with medium magnification. Textural characteristics of the catalysts were determined from adsorption–desorption isotherms of nitrogen measured at 77 K by using an automatic volumetric device ASAP 2400 (Micrometritics). The specific surface area was calculated by the standard Brunauer–Emmett–Teller (BET) method. The mean pore diameter and total pore volume were obtained by Barrett–Joyner–Halenda (BJH) analysis. Thermal analysis was conducted using an STA 449 Jupiter instrument (NETZSCH). The sample (40 mg) in a corundum crucible was heated from 25 to 600 °C (ramping 10 °C min^{-1}) under a flow of air. As a reference sample, calcined silica was used. The simultaneous TG–DSC–MS measurement was performed in an apparatus consisting of a STA 449 F1 Jupiter thermal analyzer and a QMS 403D Aëolos quadrupole mass spectrometer (NETZSCH, Germany). The measurements were made in a "synthetic air" flow (80 vol% Ar and 20 vol% O_2) in the temperature range of 30–800 °C using the heating rate of 10 °C min^{-1}, the gas flow rate of 25 mL min^{-1} and open Al_2O_3 crucibles. The sample weight is 25 mg.

2.4 Hydrogenation Procedure

Hydrogenation of 3-NS in toluene was performed under continuous-flow conditions in an H-Cube Pro™ setup (Thalesnano, Hungary) equipped with a module for automatic control of operational parameters (reaction temperature and pressure, flow rates of liquid feed and hydrogen). The liquid feed was introduced into the reactor by an HPLC pump in up-flow mode after mixing with the hydrogen flow, generated by a built-in electrolytic cell. The hydrogen pressure was maintained at the set-point level by means of automated back pressure regulator. The fixed bed cartridge-like reactors of CatCart®30 with an inner diameter of 4.0 mm and length of 30 mm (volume 0.38 cm^3) were used in the experiments. A more detailed description of the H-Cube Pro™ setup has been published elsewhere [25, 30].

Before the experiment, the cartridge containing the catalyst (0.185 g of 250–500 µm particles) was installed in a heater unit, and the mixture of pure solvent with hydrogen was fed to the reactor until the required reaction parameters (temperature, pressure, flow rates of hydrogen and liquid feed) were reached. It takes about 10 min. Afterwards, the inlet was switched to the flask with the 0.035–0.1 M stock solution of 3-NS in toluene containing *n*-decane as the internal GC standard. This moment was chosen as the starting point of the reaction. The catalytic tests were carried out at 70 °C, 1.0 MPa hydrogen pressure, solution and hydrogen feed rates of 0.5 and 60 mL min^{-1}, respectively. As a result of special tests, we found early that there is no influence of external or internal mass transfer limitations under the conditions used [12]. The first sample of liquid products was collected 30 min after feeding of the substrate; the following samples were taken every 30 min thereafter. A fresh catalyst sample was used for each catalytic run.

After the reaction was finished, the reaction flow (mixture of H_2 and the solution of 3-NS in toluene) was switched to the flow of pure toluene (0.5 mL min^{-1}), and washing of the catalyst was proceeding at the reaction temperature during 30 min. After the reactor was cooled to room temperature, the catalyst was withdrawn carefully out of the cartridge and divided into three equal samples taken at the reactor inlet, at the middle part of the reactor, and at the reactor outlet. To remove toluene and to prepare the catalyst for the further characterization, each sample was placed in the vacuum heat chamber at room temperature, evacuated to 5 mbar and then slowly heated up to 80 °C with the subsequent drying at this temperature for 3 h.

Reaction products were identified by GC–MS using an Agilent 7000B Triple Quad System. The concentrations of substrate and products were measured with GC (Agilent 6890 N instrument with a 19091S-416 HP 5-MS capillary column of 60.0 m × 320 µm × 0.25 µm in size). The conversion of 3-NS, X (%), and the selectivity, S_i (%) calculated by using Equations (1) and (2), respectively:

$$X = \left(1 - C_{3NS}/C^{0}_{3NS}\right) \times 100\%, \quad (1)$$

$$S_i = \frac{C_i}{\sum C_j} \times 100\% \quad (2)$$

where C^{0}_{3NS} and C_{3NS} are the inlet and outlet concentrations of 3-NS, respectively, C_i is the outlet concentration of the determined product; ΣC_j is the total concentration of reaction products. The error of determination of 3-NS conversion and the selectivity to 3-VA is ±1–2%.

3 Results and Discussion

3.1 Experimental Results of 3-NS Hydrogenation

The Au/Al_2O_3 catalysts with the mean diameters of Au nanoparticles ranging from 2.1 to 5.7 nm were investigated in the fixed bed flow reactor in the liquid phase hydrogenation of the 3-NS. The physico-chemical characteristics and catalytic properties of the different samples are presented in the Table 1. The products typical of 3-NS hydrogenation over the Au/Al_2O_3 catalysts are shown in Scheme 1. In addition to 3-vinylaniline (3-VA), undesired 3-vinylnitrosobenzene (3-VNSB), 3-ethylaniline (3-EA) and 3-ethylnitrobenzene (formed in trace amounts) were observed among the reaction products. The conversion of 3-NS can proceed via two routes, i.e., through the desired 3-vinylaniline generation, or via the 3-nitrostyrene hydrogenation to 3-ethylnitrobenzene leading further to 3-EA as the fully hydrogenated product [18]. No one of any previously reported [3, 5] by-products, which were formed during hydrogenation of nitrobenzenes to anilines such as benzylhydroxylamines, azoxybenzenes, azobenzenes and hydrazobenzenes, were detected in our experiments.

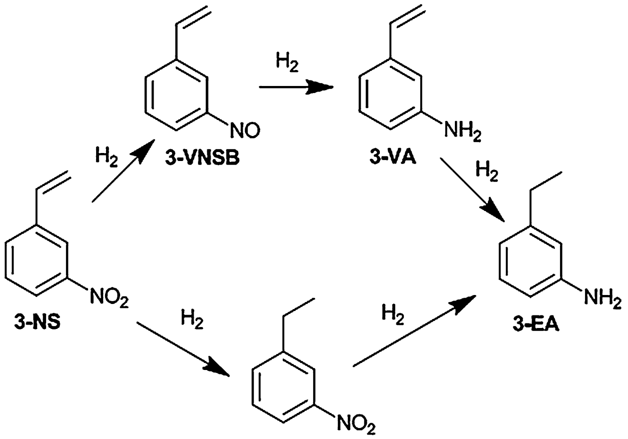

Scheme 1 Reaction pathway for the hydrogenation of 3-nitrosterene (3-NS) to the products: 3-vinylnitrosobenzene (3-VNSB), 3-vinylaniline (3-VA) and 3-ethylaniline (3-EA)

The data presented in Table 1 let us to see, that the catalyst with the mean diameter of the Au nanoparticles (d_l) equal to 2.1 nm displays the highest activity in terms of 3-NS conversion. The increase in the mean diameter of the Au particles to 2.8 nm leads to a drop in the catalytic activity. The catalyst with the highest mean diameter of the nanoparticles (5.7 nm) shows a significantly lower activity in comparison with the other samples. These results are in agreement with published data that indicates an increase of the catalytic activity of Au/Al_2O_3 catalysts in the chemoselective hydrogenation of nitroarenes with the decrease of gold particle size to less than 3 nm [5, 11, 21]. On the other hand, the selectivity towards 3-VA is practically unaffected by the size of the gold nanoparticles (Table 1).

In accordance with the obtained results, the Au/Al_2O_3-2.1 catalyst with the mean particle sizes of 2.1 ± 0.4 nm was chosen for the further study of the liquid-phase 3-NS hydrogenation. Figure 1 illustrates the TEM image for the Au/Al_2O_3-2.1 catalyst. The small black dots represent the metal gold particles up to 3.5 nm in diameter. TEM data shows mainly Au particles of 1.5–2.5 nm in diameter; but there are also a few smaller (d_i = 1.0–1.5 nm) and larger (d_i = 2.5–3.5 nm) particles. The particle size distribution has a maximum at approximately 2 nm ($d_l = 2.1$ nm) with a standard deviation (σ) equal to 0.4.

Figure 2 shows the experimental results of time-on-stream dependence of the 3-nitrostyrene conversion at the different initial concentration of 3-NS in toluene: 0.035, 0.05, 0.075, and 0.1 M. It is seen that increase in the 3-NS concentration in the reaction mixture leads to a sharper decrease in the reagent conversion with time-on stream and, as a result, to the faster catalyst deactivation.

3.2 Modeling of Catalyst Deactivation

The rate of the first-order reaction over the fresh catalyst without deactivation ($r_o(C,T)$) can be presented by the following equation:

Table 1 Effect of the mean Au particle size on 3-nitrostyrene conversion and product selectivity

Entry	Catalyst	T_{calc} (°C)[a]	Au (%)	$d_l \pm \sigma$ (nm)	*X* (%)	*S* (%)		
						3-VA	3-VNSB	3-EA
1	Au/Al_2O_3-2.1	400	1.85	2.1 ± 0.4	94	95	2	3
2	Au/Al_2O_3-2.8	600	1.82	2.8 ± 0.6	86	93	3	4
3	Au/Al_2O_3-5.7	800	1.85	5.7 ± 1.5	27	96	3	1

3-nitrostyrene (0.05 M), $T = 70$ °C, $p(H_2) = 1.0$ MPa. The performance of the catalysts was evaluated by averaging the 2 samples taken at 30–33 min and 33–36 min after the start of the experiment

[a] Calcination temperature

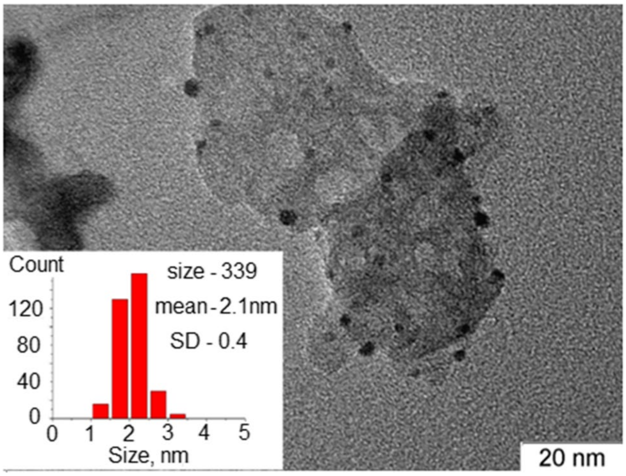

Fig. 1 TEM data of the fresh Au/Al_2O_3-2.1 catalyst

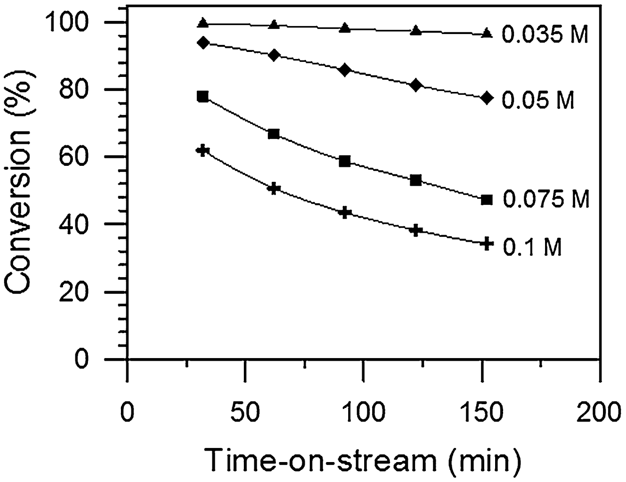

Fig. 2 Time dependence of 3-NS conversion over the Au/Al_2O_3-2.1 catalyst at different initial concentration (T = 70 °C; $p(H_2) = 1.0$ MPa)

$$r_0(C,\ T) = k(T) \times C_{3NS}, \tag{3}$$

where *k(T)* is the first-order rate constant. To take into account the influence of the catalyst deactivation on the reaction performance, a so-called "separable deactivation kinetics" approach is usually applied [31, 32]. In this approach, the rate of the catalytic reaction is expressed as a superposition of the function of the initial reaction rate of the fresh catalyst and a function characterizing the change of the catalyst activity by deactivation.

The kinetic model of 3-NS hydrogenation expresses the reaction rate as the function of the main reaction kinetics (Eq. 3) and a function of Φ that is related to the current catalytic activity:

$$r(C,\ T, t) = r_0(C,\ T) \times \Phi\left(C^0_{3NS},\ t\right), \tag{4}$$

where $\Phi\ (C_{3NS}{}^{0}, t)$ is the empirical expression also called "relative activity" or "activity function", which depends on the inlet 3-NS concentration and time-on-stream.

The activity function is defined as the ratio of the current reaction rate *r(t)* and a reaction rate r_0 at the initial period of the process, $r(t)_{t}{\rightarrow}_{0} = r_0$:

$$\Phi(t) = r(t)/r_0 = k(t)/k_0 \tag{5}$$

When the catalyst deactivation begins, the activity function $\Phi(t)$ decreases with time-on-stream.

In the absence of knowledge on the detailed mechanism of the active site deactivation a wide range of empirical correlations is used for catalyst deactivation modeling [33]. On the basis of experimental observations, Froment and Bischoff [34] proposed three main types of activity function, as follows: linear $\Phi_1 = 1-\gamma t$, exponential $\Phi_2 = \exp(-\gamma t)$, and hyperbolic $\Phi_3 = \Phi_1{}^{-1} = (1-\gamma t)^{-1}$, where γ—the empirical deactivation constant (min^{-1}).

The dependencies of the activity function on time-on-stream at different $C_{3NS}{}^{0}$ values are non-linear in our case; therefore, the Φ_1 function is not appropriate for their description. Further attempts are undertaken to describe these dependencies by using the exponential Φ_2 or hyperbolic Φ_3 function. The log-lin plots of Φ_2 versus time-on-stream for different $C_{3NS}{}^{0}$ values are not the straight lines, thus, another function should be used. Applying of the hyperbolic function results in a good description of experimental results, since the Φ_3 function depends linearly on *t* at any inlet 3-NS concentrations that have been used (Fig. 3). Based on the fitting results, the following formula can be suggested for the activity function in our case:

$$\Phi\left(C^0_{3NS},\ t\right) = \frac{1}{1 + k_d\left(C^0_{3NS}\right) \times t}, \tag{6}$$

where $k_d(C_{3NS}{}^{0})$ is parameter of deactivation depending on the inlet 3-NS concentration.

The values of k_d at different $C_{3NS}{}^{0}$ can be determined by fitting the function (6) to the Φ values calculated from the experimental data by Equations (3) and (5) (the correlation between the fitting curves and the experimental data is shown in Fig. 4).

Thus, the kinetic model consisting of Equations (4) and (6) that was developed for the reaction of 3-NS hydrogenation over the Au/Al_2O_3 catalyst fully describes the dynamics of the catalyst deactivation (Fig. 3). The dependence of the parameter of deactivation is fitted well by a parabolic function $k_d = B(C_{3NS}{}^{0})^2$ at B = ~12.7 min^{-1} (Fig. 4).

To explain the similar empirical form of Eq. (6) during isomerization of α-pinene to camphene [32] from a mechanistic point of view the authors have assumed that the formation of carbon deposits and deactivation of the Au/Al_2O_3 catalysts occur as a result of interaction between two adsorbed molecules of the reagent. Taking into account this

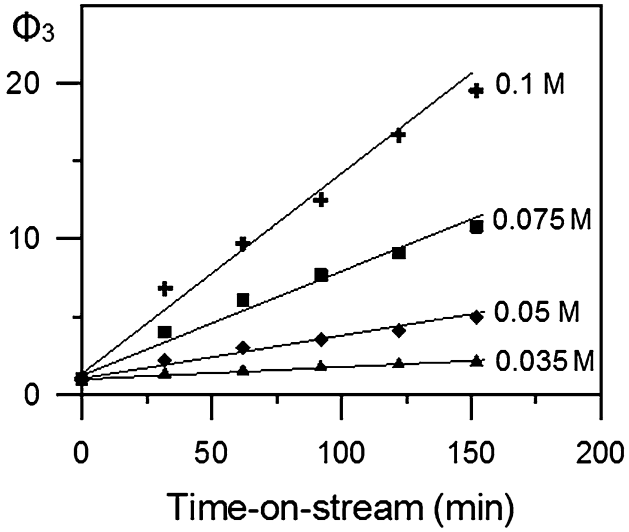

Fig. 3 Time dependence of activity function Φ_3 at different inlet concentrations of 3-NS. The symbols represent Φ_3 values calculated from the experimental data by Eqs. (3) and (5) in linear scale

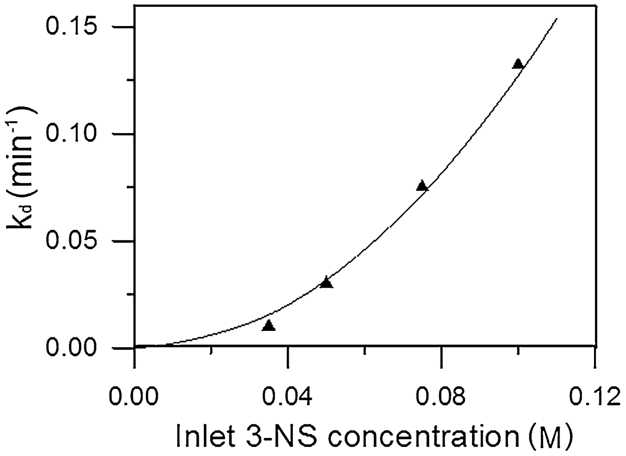

Fig. 4 Dependence of deactivation parameter (k_d) as a function of inlet 3-NS concentration

consideration, we can speculate, that in our case reagent (3-NS) or the intermediates formed on the initial stages of reaction are responsible for the formation of carbon deposits on the catalysts surface. In order to examine this speculation, the analysis of the spent catalysts taken from the different part of reactor (inlet, middle part, and outlet) is performed.

3.3 Study of the Spent Catalysts

To elucidate the impact of the different factors on the catalyst deactivation we compared the gold content, the mean particle size of gold nanoparticles, textural properties, and the carbonaceous deposition content in the fresh and spent Au/Al_2O_3-2.1 catalysts using XRF, TEM, low-temperature nitrogen adsorption and thermal analysis, respectively. Analysis of Au content, particle size, and carbon content was done for the catalyst samples tested in the reaction at the different initial concentrations of 3-nitrostyrene in toluene, 0.035, 0.05, 0.075, and 0.1 M (Fig. 2). The characteristics of the spent catalyst used in the experiment with the highest 3-NS concentration are provided in the Table 2.

TEM data of the Au/Al_2O_3 samples taken at the reactor inlet and outlet after 3-nitrostyrene (0.1 M) hydrogenation at 70 °C are shown in Fig. 5. The comparison of the mean particle size of gold in the catalysts taken after reaction with that in the fresh catalyst has not elucidated noticeable enlargement of the gold particles in any part of the reactor. An increase in the d_l value for Au particles, which was observed early after two successive catalytic runs in the 3-NS hydrogenation [12], is most likely to be caused by the intermediate regeneration of the Au/Al_2O_3 catalyst in air flow at 400 °C.

Thus, the comparison of characteristics of the fresh and spent catalysts allows us to conclude that Au content, Au particle size, and textural properties of Au/Al_2O_3 catalyst have not been changed visibly after 2.5 h on-stream even after experiments using the highest concentration of reagent (Table 2). This observation agrees with the results of the investigation of gas-phase hydrogenation of 4-CNB to 4-chloroaniline in a continuous flow fixed bed reactor over the Au/Al_2O_3 catalyst [19]. Authors have not detected any noticeable changes in the textural properties or the mean size of gold particles and suggested that the formation of carbonaceous deposits is the main reason for the Au/Al_2O_3 catalyst deactivation.

In order to evaluate the contents of carbonaceous deposits, TG-DTA analysis of the fresh and spent catalysts was performed in air atmosphere. The samples of the Au/Al_2O_3-2.1 catalyst taken from the different parts of reactor (inlet, middle part and outlet) after experiments with various initial concentrations of 3-NS were examined to evaluate the influence of 3-NS concentration on the carbon content and elucidate the allocation of carbon deposition along the reactor length. TG/DTG results for the fresh Au/Al_2O_3 catalyst are presented in Fig. 6a. The differential thermogravimetric (DTG) curve exhibits the sharp peak with a maximum at about 90 °C, which is explained by the removal of physically adsorbed water. Additionally, the slow weight loss is observed at a temperature higher than 200 °C, which is usually ascribed to the gradual removal of residual hydroxyl groups from the matrix of γ-alumina. The DTA (data not shown) and DTG curves of the fresh sample show no signs of any exothermal reaction (Fig. 6a).

Figure 6b displays the DTG curves of the samples of the Au/Al_2O_3-2.1 catalyst taken from the different parts of the reactor after experiment using the solution with the

Table 2 Physico-chemical characteristics of the fresh and spent Au/Al_2O_3-2.1 catalyst

	Fresh	Spent[a]
Content of Au (wt%)	1.85	1.82
Mean particle size (d_l) (nm)	2.1 ± 0.4	1.8 ± 0.4[b], 1.7 ± 0.4[c]
BET specific surface area ($m^2\ g^{-1}$)	215[d], 197	194[e]
Total pore volume ($cm^3\ g^{-1}$)	0.61[d], 0.58	0.56[e]
Mean pore diameter (nm)	9.6[d], 9.4	9.3[e]

[a] After 2.5 h on-stream in toluene at 70 °C, $p(H_2) = 1.0$ MPa, 3-nitrostyrene (0.1 M)

[b] Reactor inlet

[c] Reactor outlet

[d] γ-Al_2O_3 support

[e] Averaged catalytic sample

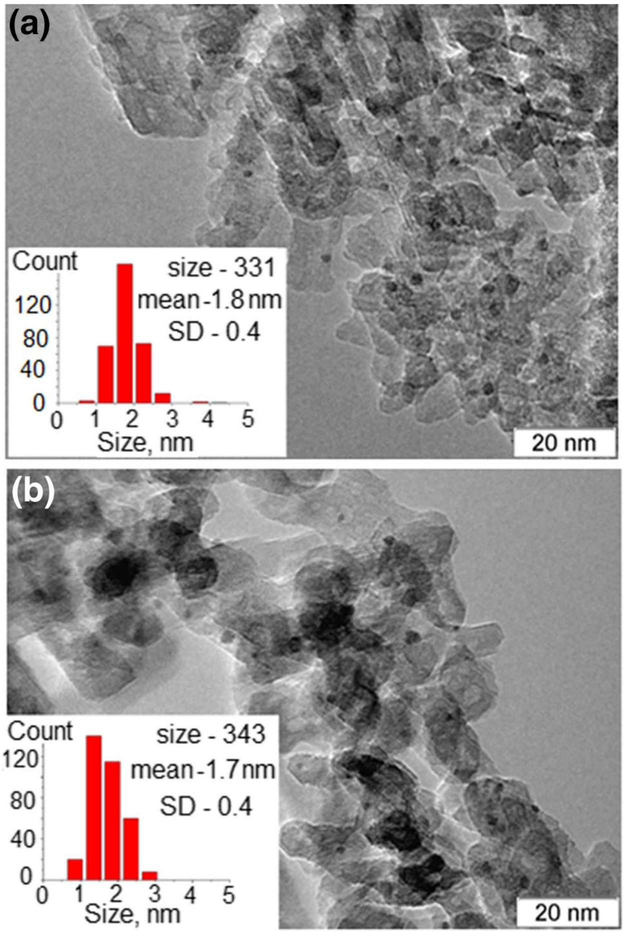

Fig. 5 TEM data of the Au/Al_2O_3-2.1 catalyst after testing for 3-NS hydrogenation at 70 °C, C = 0.1 M, $p(H_2) = 1.0$ MPa. **a** Reactor inlet, **b** reactor outlet

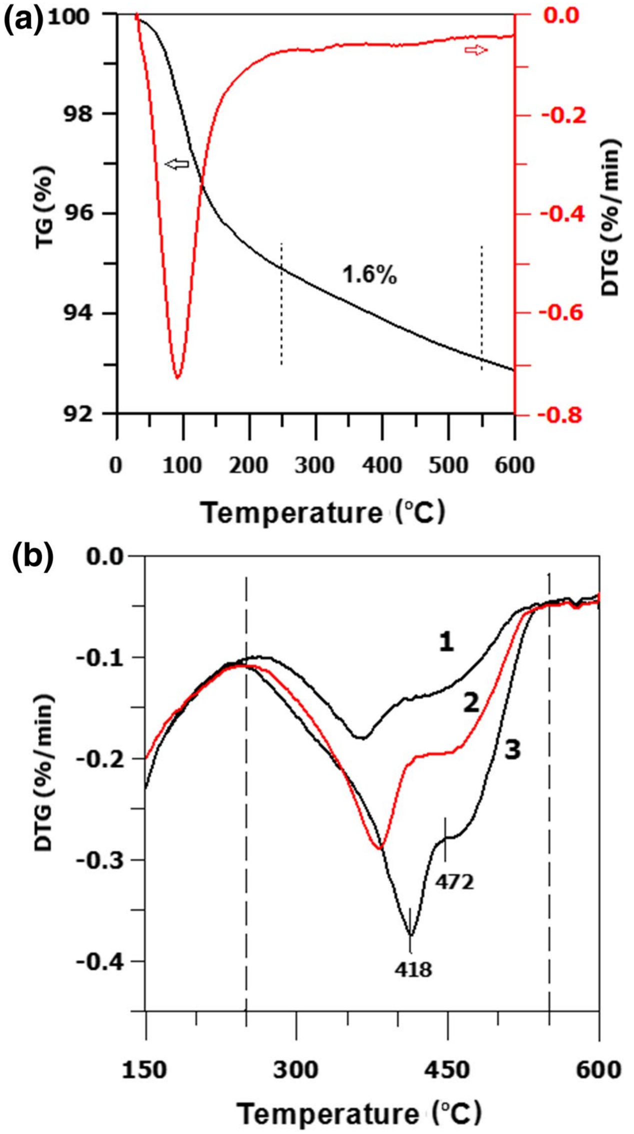

Fig. 6 **a** TG/DTG curves of the fresh Au/Al_2O_3-2.1 catalyst; **b** DTG curves of the samples of the Au/Al_2O_3-2.1 catalyst after testing for 3-NS hydrogenation at 70 °C (C = 0.1 M): at reactor outlet (*1*), at middle part of reactor (*2*), and at reactor inlet (*3*)

initial concentration of 3-NS equal to 0.1 M. For these samples, the DTG curves exhibit two weight loss regions: the first is caused by the removal of adsorbed water (not shown) and the second (250–520 °C) could be explained by combustion of carbonaceous species on the catalyst surface that was confirmed by TG–DSC–MS data [32, 35]. The position of the exothermic peak on the DSC curve as well as carbon dioxide, nitrogen monoxide and water peaks on the MS curves corresponds to weight loss region on the DTG curves (Figs. 6b, 7). Thus, carbon deposits containing some amount of hydrogen and nitrogen are formed on the catalyst surface during the liquid-phase 3-NS hydrogenation.

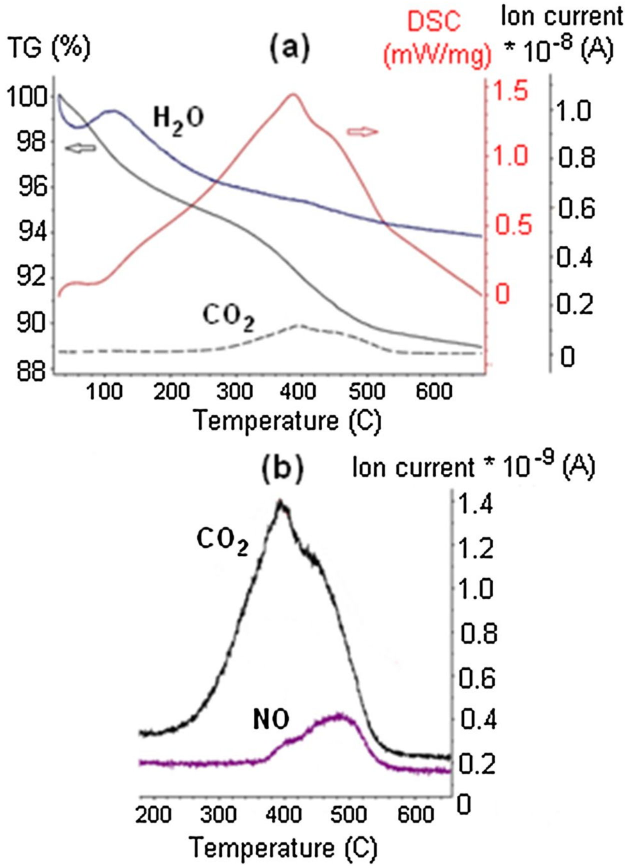

Fig. 7 TG–DSC–MS data for the sample of the Au/Al_2O_3-2.1 catalyst (at middle part of reactor) after testing for 3-NS hydrogenation at 70 °C, C = 0.1 M

Figure 8 shows the dependence of carbonaceous deposit content at the reactor inlet, at the middle part of the reactor, and at the reactor outlet on the initial 3-NS concentration. The amount of carbon deposits in the catalyst was determined as follows: the corresponding weight loss of the fresh catalyst equal to 1.6% was subtracted from the amount of relative weight loss of the spent catalyst in the temperature range 250–520 °C (TG curves). It is clearly seen, that the content of carbonaceous deposits in the samples during the same time of reaction is increased with the increasing of the initial 3-NS concentration (Fig. 8). Besides, the content of the carbonaceous deposits on the catalyst surface at the inlet of the reactor is higher than that at the outlet. This observation leads us to conclusion that the carbon-containing deposits on the surface of the catalyst are obtained starting from 3-nitrostyrene or the intermediates formed at the initial stages of 3-nitrostyrene hydrogenation to 3-vinylaniline.

The conversion of 3-NS was not observed under reaction conditions (T = 70 °C, $p(H_2) = 1.0$ MPa) over Al_2O_3. If nitrogen was used instead of hydrogen, 3-NS also was not

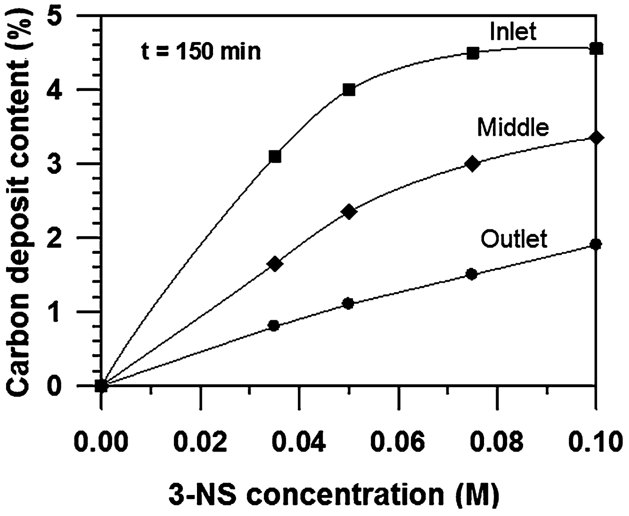

Fig. 8 Effect of the initial 3-NS concentration on carbon deposit contents in the catalyst samples at the different parts of reactor. Time of reaction run is 150 min, T = 70 °C

converted over Au/Al_2O_3 catalyst at the same conditions. In both of the above examples, no carbon deposits were found on the catalyst surface after the experiment. Therefore it is unlikely that 3-nitrostyrene is a source of carbon deposits. In accordance with the generally accepted mechanism the reduction of nitroarenes to anilines occurs in several steps, either by the direct route via nitroso and hydroxylamine intermediates or via a condensation route [3, 5]. In our case, during a hydrogenation of 3-NS to 3-VA over Au/Al_2O_3 catalyst, only the 3-vinylnitrosobenzene formed in the first stage of reaction was detected in solution. Taking into account that nitrosobenzene can be strongly coordinated via –N=O group to the surface of oxides containing Lewis acidic sites [36, 37], we suggest 3-vinylnitrosobenzene to be the main source of carbon deposits. Thus, the following scheme for the catalyst deactivation can be proposed (Scheme 2).

4 Conclusions

Dynamics of the Au/Al_2O_3 catalyst deactivation in liquid-phase chemoselective hydrogenation of 3-nitrostyrene was studied in the fixed bed flow reactor. It was found that formation of carbon-based deposits was the main reason of deactivation of the Au/Al_2O_3 catalyst, while the leaching of Au from the catalyst surface and increase in the mean gold particle size were not detected. The content of the carbonaceous deposits on the spent catalyst at the inlet of the reactor is higher than that at the outlet and increases as the initial concentration of 3-NS grows. The character of carbonaceous deposits allocation and analysis of reaction

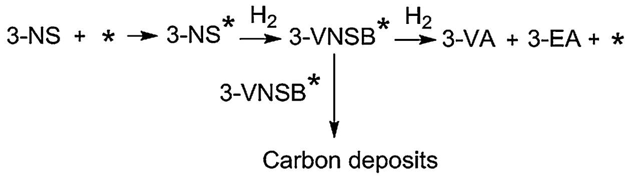

Scheme 2 Proposed mechanism of carbon deposits formation during the selective liquid-phase hydrogenation of 3-nitrostyrene over Au/Al_2O_3 catalyst (where *asterisk* is the surface active site of the catalyst)

products point out to 3-vinylnitrosobenzene as the main source of the Au/Al_2O_3 catalyst deactivation coinciding with the speculation arising from the kinetic modeling.

Acknowledgements The authors thank Russian Science Foundation (Grant 14-23-00146) for the financial support of this study.

References

1. Downing RS, Kunkeler PJ, van Bekkum H (1997) Catal Today 37:121–136
2. Blaser H-U (2006) Science 313:312–313
3. Blaser H-U, Steiner H, Studer M (2009) ChemCatChem 1:210–221
4. Ananikov VP, Khemchyan LL, Ivanova YuV, Bukhtiyarov VI, Sorokin AM, Prosvirin IP, Vatsadze SZ, Medvedko AV, Nuriev VN, Dilman AD, Levin VV, Koptyug IV, Kovtunov KV, Zhivonitko VV, Likholobov VA, Romanenko AV, Simonov PA, Nenajdenko VG, Shmatova OI, Muzalevskiy VM, Nechaev MS, Asachenko AF, Morozov OS, Dzhevakov PB, Osipov SN, Vorobyeva DV, Topchiy MA, Zotova MA, Ponomarenko SA, Borshchev OV, Luponosov YuN, Rempel AA, Valeeva AA, Stakheev AYu, Turova OV, Mashkovsky IS, Sysolyatin SV, Malykhin VV, Bukhtiyarova GA, Terentev AO, Krylov IB (2014) Russ Chem Rev 83:885–985
5. Cardenas-Lizana F, Keane MA (2013) J Mater Sci 48:543–564
6. Serna P, Boronat M, Corma A (2011) Top Catal 54:439–446
7. Corma A, Serna P, Concepcion P, Calvino JJ (2008) J Am Chem Soc 130:8748–8753
8. Motoyama Y, Lee Y, Tsuji K, Yoon S-H, Mochida I, Nagashima H (2011) ChemCatChem 3:1578–1581
9. Corma A, Serna P (2006) Science 313:332–334
10. Boronat M, Concepcion P, Corma A, Gonzalez S, Illas F, Serna P (2007) J Am Chem Soc 129:16230–16237
11. Shimizu K, Miyamoto Y, Kawasaki T, Tanji T, Tai Y, Satsuma A (2009) J Phys Chem C 113:17803–17810
12. Nuzhdin AL, Moroz BL, Bukhtiyarova GA, Reshetnikov SI, Pyrjaev PA, Aleksandrov PV, Bukhtiyarov VI (2015) ChemPlusChem 80:1741–1749
13. Matsushima Y, Nishiyabu R, Takanashi N, Haruta M, Kimura H, Kubo Y (2012) J Mater Chem 22:24124–24131
14. Shimizu K-I, Miyamoto Y, Satsuma A (2010) J Catal 270:86–94
15. Mitsudome T, Mikami Y, Matoba M, Mizugaki T, Jitsukawa K, Kaneda K (2012) Angew Chem Int Ed 51:136–139
16. Reis PM, Royo B (2009) Tetrahedron Lett 50:949–952
17. Serna P, Concepcion P, Corma A (2009) J Catal 265:19–25
18. Yarulin A, Berguerand C, Yuranov I, Cardenas-Lizana F, Prokopyeva I, Kiwi-Minsker L (2015) J Catal 321:7–12
19. Cardenas-Lizana F, Lamey D, Li M, Keane MA, Kiwi-Minsker L (2014) Chem Eng J 255:695–704
20. He D, Shi H, Wu Y, Xu B-Q (2007) Green Chem 9:849–851
21. Hartfelder U, Kartusch C, Makosch M, Rovezzi M, Sa J, van Bokhoven JA (2013) Catal Sci Technol 3:454–461
22. Wang X, Perret N, Delgado JJ, Blanco G, Chen X, Olmos CM, Bernal S, Keane MA (2013) J Phys Chem C 117:994–1005
23. Perret N, Wang X, Delannoy L, Potvin C, Louis C, Keane MA (2012) J Catal 286:172–183
24. Wang XD, Perret N, Keane MA (2012) Chem Eng J 210:103–113
25. Irfan M, Glasnov TN, Kappe CO (2011) ChemSusChem 4:300–316
26. Hessel V (2009) Chem Eng Technol 32:1655–1681
27. Baxendale IR, Brocken L, Mallia CJ (2013) Green Process Synth 2:211–230
28. Wiles C, Watts P (2014) Green Chem 16:55–62
29. Moroz BL, Pyrjaev PA, Zaikovskii VI, Bukhtiyarov VI (2009) Catal Today 144:292–305
30. Jones RV, Godorhazy L, Varga N, Szalay D, Urge L, Darvas F (2006) J Comb Chem 8:110–116
31. Froment GF, Bischoff KB (1961) Chem Eng Sci 16:189–201
32. Solkina YuS, Reshetnikov SI, Estrada M, Simakov AV, Murzin DY, Simakova IL (2011) Chem Eng J 176–177:42–48
33. Satterfield CN (1984) Heterogeneous catalysis in practice. McGraw-Hill Book Company, New York
34. Froment GF, Bischoff KB (1979) Chemical reactor analysis and design. Wiley, New York
35. Nuzhdin AL, Artiukha EA, Bukhtiyarova GA, Zaytsev SYu, Plyusnin PE, Shubin YuV, Bukhtiyarov VI (2016) RSC Adv 6:88366–88372
36. Meijers S, Ponec V (1996) J Catal 160:1–9
37. Richner G, van Bokhoven JA, Neuhold Y-M, Makosch M, Hungerbuchler K (2011) Phys Chem Chem Phys 13:12463–12471